Proceedings of Global Power and Propulsion Society
ISSN-Nr: 2504-4400
GPPS Chania24
September 4-6, 2024
www.gpps.global

GPPS-TC-2024-077

STEAM COMPRESSOR FLOW SIMULATION CLOSE TO THE SATURATION LINE USING NON-IDEAL GAS MODEL

Bojan Kajasa
German Aerospace Center (DLR)
Bojan.Kajasa@dlr.de
Zittau, Saxony, Germany

Michael Lockan
German Aerospace Center (DLR)
Michael.Lockan@dlr.de
Cottbus, Brandenburg, Germany

Eberhard Nicke
German Aerospace Center (DLR)
Eberhard.Nicke@dlr.de
Zittau, Saxony, Germany

ABSTRACT

The heat supply for industrial production in the medium temperature range can be provided by green electricity to substitute fossil energy sources. Here the use of High-Temperature Heat-Pumps (HTHP) is a very promising technology to reduce significantly the power demand. The operation of the HTHP require a dedicated design of the turbomachinary used within. For the working medium low superheated steam a well-adapted non-ideal gas model is required for the 3D-RANS simulations. In addition to the temperature dependence, a model adaptation is developed to include the pressure dependence of the gas properties within the CFD simulations. A polytropic state change in temperature and pressure is assumed and determined for the heat capacity along the estimated state change as function of this two gas properties. This polynomial function is developed and applied and only valid between the assumed inlet and outlet state of the compressor stage. A comparison is performed between the calorically and thermally perfect gas model close to a non-ideal gas model, for different operation points. The dependency of the assumed polytropic state change on the developed polynomial function will be shown. The method will be used in the centrifugal compressor design and will be a part of the process chain.

INTRODUCTION

The impact of climate change is a major challenge for coming decades and the negative consequences on humanity requires a new approach to the effects of global warming (Pörtner, 2022). The impact of industries use of fossil fuels for production processes can no longer be ignored. In order to reduce the industries greenhouse gas emissions at the same production intensity, these energy sources had to be replaced. The use of high-temperature heat pumps could be a key technology in providing the process heat required by industry with sustainable energy. A HTHP can operate by considering the Rankine thermodynamic cycle based on steam as the working medium. The advantage of this cycle is that it provides a significant ratio of electrical power input to heat output (Arpagaus et al., 2018). This ratio, definded as Coefficient of Performance (COP) is highly dependent on the temperature increase generated by the HTHP. The turbo-compressor is a promising component to generate this reasonable temperature rise in the targeted output range. To achieve this, a compression system of a small number of high-performance centrifugal turbo compressors followed by an inter-stage cooler is used in HTHPs. The advantage over the axial turbo compressors commonly used in aviation is that fewer stages are required for the same performance ratio (Casey and Robinson, 2021). On the other hand, these centrifugal compressors operate with steam as the working medium and relatively small operating ranges with mass flow rates of 0.2 kg/s to 0.5 kg/s for HTHPs with a heat output up to 1 MW_{th}. The inlet conditions of the compressor stages are defined by low superheated steam in a wide range of inlet temperatures (100 °C to 180 °C). It is therefore essential that the simulations of these turbo compressors are accurate in comparison the real physical effects. As the mean line method provides an initial blade geometry, computational fluid dynamics (CFD) methods are used to improve the design of a centrifugal turbo compressor. The CFD simulations use solvers that solve 3D RANS differential equations, with turbulence models used to solve the closure problem of these equations (Ferziger and Perić, 2002). The main experience for CFD simulations based on air as the working medium and turbomachinery fluid dynamics is generated with the comprehensive in-house flow solver Turbomachinery Research

Aerodynamic Computational Environment (TRACE) from the German Aerospace Center (DLR) Institute for Propulsion Technology (Franke et al., 2005). For this reason, most solvers implement the calorically perfect gas model, where the heat capacity of the gas is independent of pressure and temperature. This ideal gas model has only limited and simplified applicability for the design of a centrifugal compressor for a Rankine-based HTHP. The heat capacity of steam is very sensitive to temperature in the gas phase near the saturation line. A first step forward to take this into account is the use of a thermally perfect gas model where a temperature-dependent and pressure-independent heat capacity is modelled (Fedkiw et al., 1996).

In a previous work, an approach for the determination of the seven NASA polynomial coefficients for a thermally perfect gas model was developed (Kajasa et al., 2023). The gas properties are determined from steam tables (Grigull et al., 2012). This provides a CFD simulation with steam as the working fluid with a temperature dependence of the heat capacity along a constant pressure progression. Nevertheless, this modelling only represents the gas properties at a constant pressure progression. As there is a pressure increase within the compressor stage, a temperature and pressure dependency of the gas properties must be modelled in the CFD simulations with the gas model used. This paper presents an approach for considering temperature and pressure dependence and the obtained results. The here proposed approach analog to the thermally perfect gas model is expected to provide a similar computing time as a calorically perfect gas model. This is particularly suitable for optimizations in the turbomachine design process.

METHODOLOGY

To investigate the approach with CFD simulations, the TRACE flow solver is chosen. TRACE is a structured and unstructured flow solver with non-linear solvers in the time and frequency domains (Franke et al., 2005). For the implemented thermally perfect gas model in TRACE, the thermochemical data are based on the GRI-Mech optimised mechanism to model natural gas combustion (Frenklach et al., n.d.). As these are different from the gas properties in the steam tables, an adjustment of the seven polynomial coefficients is required. First, the gas properties from the steam tables used for the investigation are examined. The interpolation for determining the seven polynomial coefficients, computed from these gas properties, is subsequently explained. The characteristic of the polynomial coefficient function for a temperature and pressure-dependent representation of the gas properties is compared as follows. At the end, the methodology concludes with a mesh sensitivity study for three different grid qualities.

Gas Properties from IAPWS for Water and Steam

The gas properties shown and used in this paper are based on the definition from the IAPWS Industrial Formulation 1997 for the Thermodynamic Properties of Water and Steam (Wagner et al., 2000). This representation of the gas properties is adequate for an investigation of the gas phase and a pressure range of 3 to 10 bar used in this paper. As the values for the specific heat capacity as a function of pressure and temperature are determined by the open source library CoolProp (Bell et al., 2014), where the IAPWS-97 is implemented, it is recommended to compared the values from the NIST Real Gas Model database for thermophysical properties of fluid systems. These values are computed with the NIST Chemestry Webbook (Acree and Chickos, 2023) at pressures of 3, 5, 10 bar as well at the inlet pressure of the compressor stage 3.8 bar

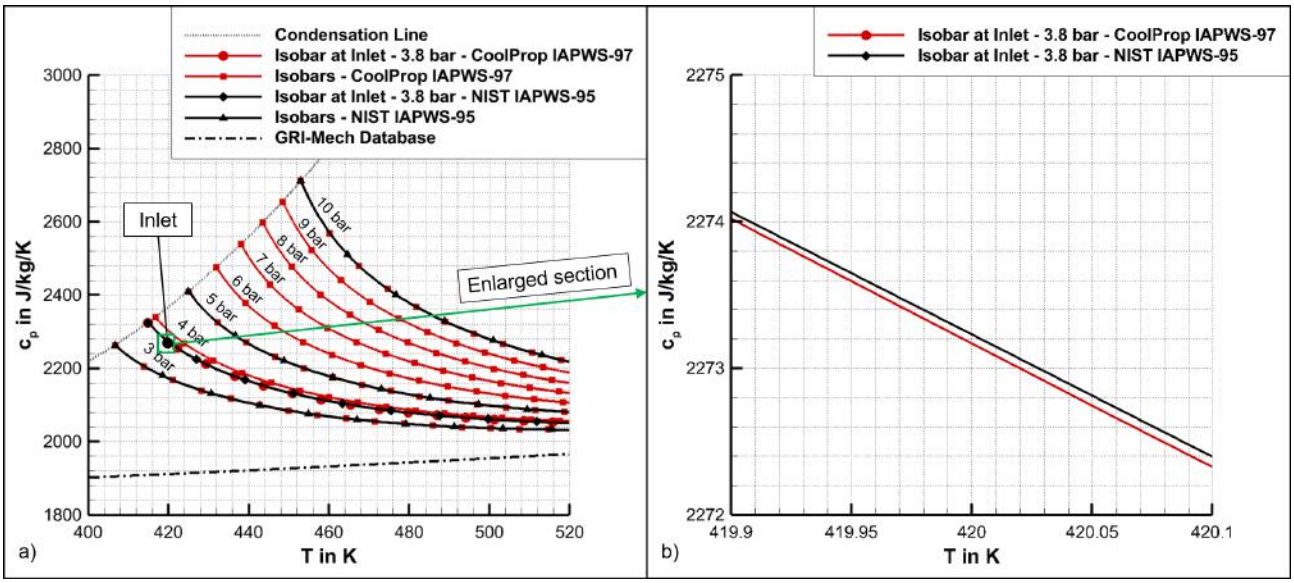

Figure 1 Steam Table at Gas Phase (a) and enlarged Section View at Inlet (b).

in a temperature range of 300 to 1000 K with a step size of 0.1 K. Compared to the NIST Real Gas Model database for water and steam, which is based on the IAPWS Formulation 1995 for the Thermodynamic Properties of Ordinary Water Substance for General and Scientific Use, the IAPWS-97 provides considerably faster computation of the gas property range. Figure 1 (a) presents the gas phase from the steam tables with isobars between 3 and 10 bar of the two formulations. In Figure 1 (b) can be demonstrated that there is no significant difference in the progression of the specific heat capacity between the CoolProp and the NIST computation. Therefore the CoolProp library provides the required gas properties for water at the gasphase and enables the development of the approach presented here for determining the seven polynomial coefficients.

Polytropic State Change Interpolation

In this section, the interpolation of the temperature-and pressure dependent progression of the specific heat capacity in the interesting pressure range is explained. In order to determine a temperature- and pressure-dependent value in the steam table, the pressure must be calculated step by step as a function of the temperature. Figure 2 (a) shows the specific heat capacity over the temperature at selected pressure values for low superheated steam based on the table (Grigull et al., 2012). The solid lines represent the isobars at 3 and 10 bar. It can be seen that the progression of the gas properties determined by the polynomial coefficients from the GRI-Mech database deviates from the physical progression. As mentioned earlier and shown in Figure 2, the flow conditions at the inlet are at a pressure of 3.8 bar and a temperature of 420 K and provides the starting point for the compression and thus interpolation. The figure is supposed to demonstrate the development of the approach of modeling temperature and pressure-dependent gas properties in the numerical flow simulation. As already mentioned above, a determination of the seven necessary polynomial coefficients at a constant pressure was carried out in the previous work (Kajasa et al., 2023). This is now enhanced by a pressure dependency resulting from the polytropic change of state within the centrifugal compressor stage. As illustrated in a thermodynamic cycle diagram for compressors, where the temperature T is plotted over the entropy s as can be seen in Figure 2 (b). In this paper the polytropic state change is modelled based on the polytropic relationship (Equation 1) combined with the polytropic efficiency:

$$\frac{T_2}{T_1} = \left(\frac{p_2}{p_1}\right)^{\frac{n-1}{n}} \tag{1}$$

The variables contained in Equation 1 are the temperature T_1 and pressure p_1 at the inlet, the temperature during polytropic compression T_2 and the pressure after compression p_2. The polytropic exponent n for steam and the mentioned inlet conditions T_1 and p_1 is calculated and is set here with a value of 1.301. As non-isentropic compression results in the real process, it is essential to consider the polytropic efficiency η_p in the following equation:

$$\eta_p = \frac{n/(n-1)}{\gamma/(\gamma-1)} \tag{2}$$

Equation 2 for the calculation of the polytropic efficiency η_p according to (Casey and Robinson, 2021), the polytropic exponent n at a real compression is related to a isentropic exponent γ of a compression without entropy change. For the approach proposed here, it is required to specify a initial value for the polytropic efficiency. The exact values are discussed in the next subsection Polynomial Coefficients. The Equation 1 and Equation 2 are used to calculate a pressure value incrementally. To perform this calculation, the following conversion is realized:

$$\frac{n-1}{n} = \frac{\gamma-1}{\gamma\eta_p} \tag{3}$$

$$n = \frac{\gamma\eta_p}{\gamma\eta_p - (\gamma-1)} \tag{4}$$

$$\frac{T_2}{T_1} = \left(\frac{p_2}{p_1}\right)^{\frac{\gamma-1}{\gamma\eta_p}} \tag{5}$$

As the pressure value is to be determined, the resulting equation is rearranged according to the pressure after incremental compression. By transforming this resulting term further, the following equation is derived to determine the pressure value:

$$p_2 = p_1 \left(\frac{\Delta T}{T_1} + 1\right)^{\frac{\gamma\eta_p}{\gamma-1}} \tag{6}$$

The pressure p_1 specified in this equation is the inlet pressure and is a constant value of 3.8 bar for each calculation. The stepwise determination of the pressure p_2 is dependent on the temperature change ΔT. The temperature is increased by 0.1 K steps. For each computation step, ΔT step is added until a pressure value for p_2 equal to or greater than 10 bar is reached. The calculation is then considered complete and 1.071 pressure values are determined for the selected step size. Using these determined pressure values and the corresponding temperature values, a correlated value for the specific heat

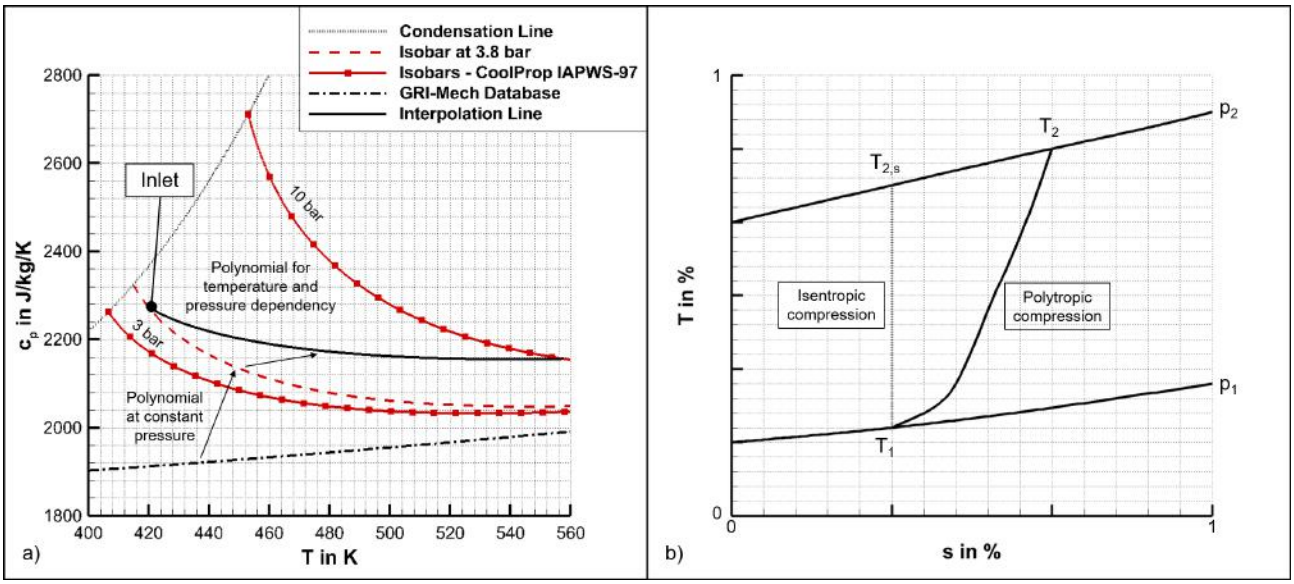

Figure 2 Steam Table at Gas Phase (a) and Thermodynamic Cycle T-s Diagram for Compressors (b).

capacity is determined with the the open-source library CoolProp (Bell et al., 2014). The progression of these determined heat capacity values is used to calculate the required seven polynomial coefficients, which are examined in the next section.

Polynomial Coefficients

As previously mentioned, similar as for the thermally perfect gas model, polynomial will be used here and so it is essential to determine the seven polynomial coefficients in order to model the gas properties of the working medium in the numerical flow simulation. The determination of these coefficients is carried out by using a polynomial regression of the previously identified heat capacity progression. The seven polynomials can be used to compute the specific heat capacity, enthalpy and entropy of the medium in the gas model. Here, only slight reference is made to the heat capacity, enthalpy and entropy by using the following equations:

$$\frac{c_p}{R} = a_1 + a_2 T + a_3 T^2 + a_4 T^3 + a_5 T^4 \tag{7}$$

$$\frac{h}{RT} = a_1 + a_2 \frac{T}{2} + a_3 \frac{T^2}{3} + a_4 \frac{T^3}{4} + a_5 \frac{T^4}{5} + a_6 \frac{1}{T} \tag{8}$$

$$\frac{s}{R} = a_1 lnT + a_2 T + a_3 \frac{T^2}{2} + a_4 \frac{T^3}{3} + a_5 \frac{T^4}{4} + a_7 \tag{9}$$

In Equation 7, the specific heat capacity c_p is determined from the polynomials a_1 to a_5. The value 461.5 J/kg/K is used for the gas constant R for steam calculated with the CoolProp library. These equations can be discussed in detail in here (Burcat and Ruscic, 2005). For this paper, 3 interpolations are initially performed at a polytropic efficiency of the centrifugal compressor stage at 60 %, 70 % and 80 %. An interpolation is also conducted at a theoretical efficiency of 100 %. However, this is only intended to illustrate the trend development in the steam table and is not considered further. The Table 1 summary of the polynomials a_1 to a_7 primarily shows the values from the GRI-Mech database known from the literature. In comparison with the values at a constant pressure of 3.8 bar, deviations in the order of magnitude of the values can be seen. The polynomial values for the three efficiencies are also entered. As the efficiency decreases, the magnitudes

Table 1 Polynomial Coefficients for Steam for the Thermally Perfect Gas Model

	a_1	a_2	a_3	a_4	a_5	a_6	a_7
GRI-Mech	4.199e+00	-2.036e-03	6.520e-06	-5.488e-09	1.772e-12	-3.029e+04	-8.490e-01
Calc. at 3.8 bar	2.211e+01	-9.684e-02	1.939e-04	-1.687e-07	5.456e-11	1.589e+03	-1.462e+02
Interp. with 80 %	1.095e+02	-8.044e-01	2.326e-03	-3.003e-06	1.459e-09	-1.515e+04	-1.439e+03
Interp. with 70 %	8.998e+01	-6.346e-01	1.779e-03	-2.226e-06	1.049e-09	-1.022e+04	-1.103e+03
Interp. with 60 %	7.159e+01	-4.787e-01	1.288e-03	-1.548e-06	7.005e-10	-6.148e+03	-8.048e+02

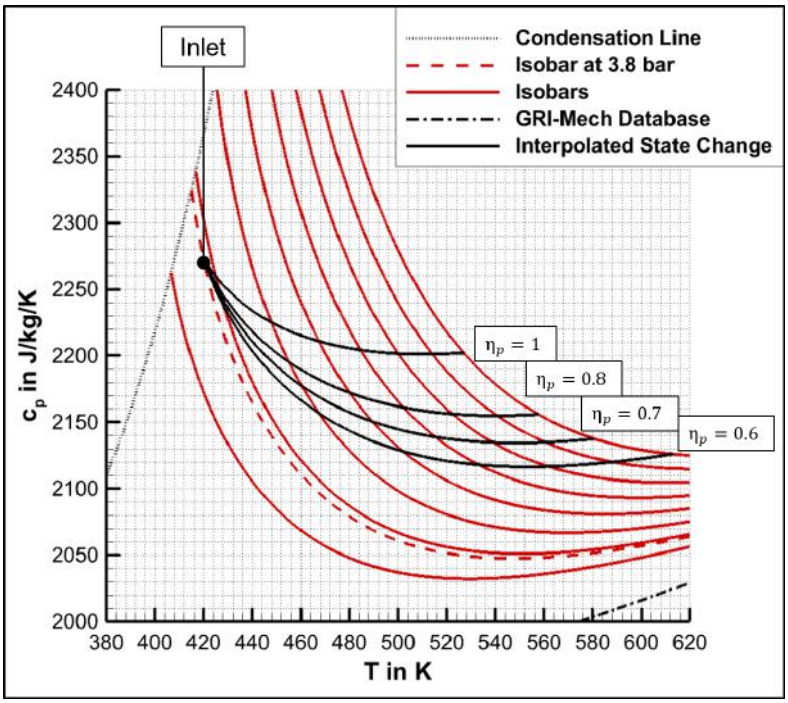

Figure 3 Steam Table at selected pressure values and Interpolation Curves .

also decrease, which can lead to a smoothing of the characteristic profile. This trend can be seen very clearly in Figure 3. All interpolations start at the specified pressure and temperature at the inlet resulting from the thermodynamic cycle calculation of the compressor stage and are 3.8 bar and 420 K. Here is how the progression of the interpolated values of the specific heat capacity decreases more gradually over the pressure increase up to 10 bar than at an isobaric development. An interpolation of 80 % results in a temperature of 555 K at 10 bar. At 60 % it is approximately 610 K.

Centrifugal Compressor Stage

This section introduces the centrifugal compressor stage used for the investigation. This stage is implemented in the Institute's pilot plant HTHP, which is currently under development. Three radial compressor stages are provided for the pressure increase and temperature lift by the HTHP, which are arranged in a low-pressure, medium-pressure and high-pressure compressor. This ensures that a pressure of up to 16 bar and a temperature of 575 K can be achieved with the three stages in row. The centrifugal compressor stage discussed in this paper is the medium-pressure stage of this HTHP. This stage is selected as the geometry has been designed and optimized for the requirements of the HTHP and is the furthest progressed in the development process of the pilot plant. To validate the numerical flow results, test runs will soon be performed on a test rig with this stage and performance map measurements will be taken. The centrifugal compressor stage investigated in this work as shown in Figure 4 consists of 19 impeller main blades, 14 diffuser blades and a symmetrical volute. The tip diameter D_2 of the impeller is 110 mm with an blade width b_2 at impeller tip of 2.8 mm. The axial length L of the impeller blades is 17.5 mm. The inlet plane of the volute is at a diameter D_4 of 180 mm. As already mentioned, the CFD solver TRACE is used for the flow simulation. The impeller and diffuser domains are meshed and simulated as a structured blade passage. The volute is meshed as a full-body unstructured mesh. Overall, a high resolution of the computational domain and a total cell count of 2,505,967. To solve the closure problem of RANS, a two-equation k-ω Menter SST turbulence model is used (Menter and Rumsey, 1994). To resolve the boundary layer at the impeller and the vaned diffuser blades and casing walls, the first cell height is defined where the Low Reynolds wall treatment can be applied to these viscous walls. The first wall coordinate y^+ in the impeller and diffuser domains is less than 1. For the volute and outlet duct, the wall function is applied to the viscous walls. Here the value of y^+ is between 20 and 50. Due to the fact that only one blade passage of the impeller and the diffuser is calculated, a mixing plane must be used between impeller and diffusor and diffusor and volute. From the thermodynamic cycle calculations, a total pressure of 3.8 bar is set at a temperature of 420 K as the inlet conditions. The speedline calculation is performed for 12 operating points and the convergence criteria are set at 0.05 % variation in mass flow, pressure ratio and efficiency within a step size of 500 iterations. The surge limit is reached with decreasing back pressures up to a value of 0.005 bar in deviation from the previously converged simulations.

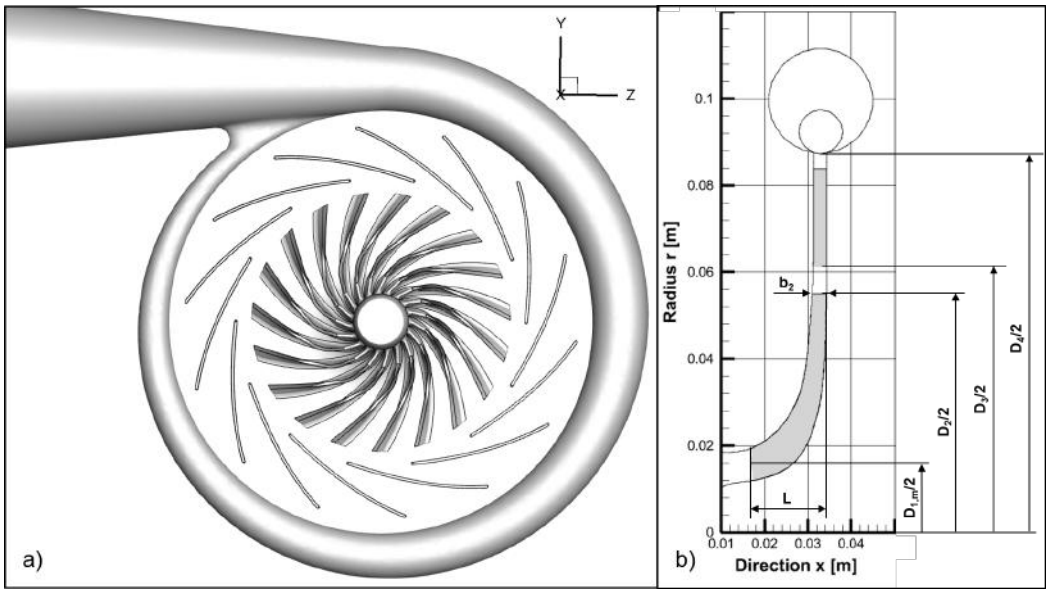

Figure 4 Centrifugal Compressor Stage (a) and Meridional Flowpath (b) Geometry.

Mesh Sensitivity

In order to check the grid resolution, a mesh sensitivity study of computational domain is performed. For this purpose, the grid is modified twice with a refinement ratio of about 1.2. The dimensions of the main blocks and the constant cell spacings close to the edges were changed to achieve a suitable simulation. Since only integer block dimensions are changed, the theoretical refinement ratio of 1.2 could not be achieved exactly for some mesh modifications. The CFD simulation is solved for each mesh. The Richardson extrapolation method is used to compare the results with a theoretical calculation on an infinitesimal fine mesh (Roache, 1994) and (Slater, 2022). The theoretical basis of the Richardson extrapolation can be described as follows:

$$E = C * h^p \tag{10}$$

where E is the error, p is the order of convergence and h is the spatial discretization. With the Taylor approximation, the value of the calculated parameter on an infinitesimally fine mesh can be calculate with:

$$f_{h=0} = f_{fine} + \frac{f_{fine} - f_{medium}}{r^p - 1} \tag{11}$$

Rearranging this Equation 11 makes it possible to determine the convergence order p with the following equation:

$$p = \frac{ln\left(\frac{f_{coarse} - f_{medium}}{f_{medium} - f_{fine}}\right)}{ln(r)} \tag{12}$$

Richardson extrapolation can be used to calculate the error between each solved mesh and the solution on the theoretical infinitesimal fine mesh. The study compares three settings for the number of cells of the overall computational domain, which are summarized in Table 2. By meshing the centrifugal compressor stage as a structured mesh topology for the impeller and vaned diffuser and unstructured meshing of the volute and the outlet tube, a degree of refinement is selected that is sufficient for the requirements of a turbomachinery flow simulation and allows the boundary layer separation to be modeled on viscous walls. For this reason, a first cell size is adjusted for all three grid configurations where the dimensionless boundary layer parameter y^+1 is less than 1 as can be seen in Table 2. The isentropic efficiencies and total pressure ratios of the three flow solutions are used to compare the refinement settings. These values are used to calculate the relative error and are applied in Equation 12. For a comparison with the Richards extrapolation, where the theoretical value for the error

Table 2 Mesh refinement with the number of cells

	coarse	medium	fine
No. of Cells	1,103,438	1,717,912	2,505,967
1^{st} Cell Size	$y^+ < 1$	$y^+ < 1$	$y^+ < 1$

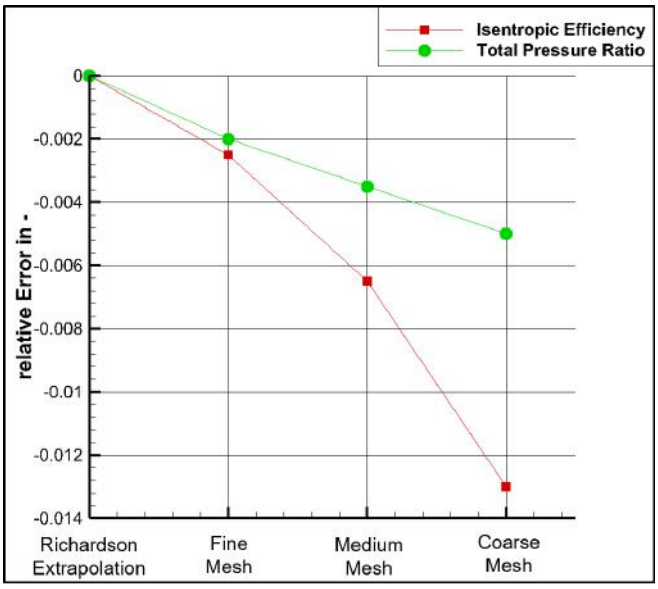

Figure 5 Richardson Extrapolation in Comparison with three different Mesh Resolutions.

equals 0, the three relative errors of the two compressor stage parameters are shown in Figure 5. First of all, it can be seen clearly that the influence of the isentropic efficiency between the three mesh qualities has a higher influence on the relative error. For the coarsest grid, this is approx. 1.3 % and at the finest setting, it is approx. 0.25 %. The influence of the total pressure ratio is minor in comparison. A relative error of approx. 5 % can be recognized for the coarse mesh and approx. 2 % for the fine mesh setting. The mesh sensitivity study demonstrates that the fine tuned mesh with 2,505,967 cells can be used for the investigations and provides adequate flow simulation solutions for the results in the following section.

RESULTS AND DISCUSSION

This section presents the results of the numerical flow simulations. The focus is on different areas of evaluation. Firstly, the performance parameters of the centrifugal compressor stage are presented and discussed. The second part is the analysis of mean line distribution through the centrifugal compressor stage. Finally, contour plots are presented at a constant blade height of 50 % and a distribution within the stage is considered. Therefore, 0D, 1D and 2D results of the numerical flow solution are used for the investigation. The simulations are performed with polynomial coefficients interpolated at an polytropoic efficiency of 60 and 80 %.

Compressor Stage Performance

To analyze the performance parameters of the compressor, a speed line is simulated and the compressor maps are visualized. Figure 6 (a) shows the total pressure ratio over the mass flow for the impeller and the overall compressor stage. The flow solutions with the thermally perfect gas model result in a 0.05 higher pressure ratio than the calculation with the ideal gas model at the design point. The presentation of the two speed lines, calculated with a polytropic efficiency of 60 and 80 %, indicates no significant deviation. The speed lines as well as the surge and choke limit distances are almost equal. The comparison between the two polynomial computations demonstrates that the solution at a constant pressure has a surge limit deviation. In either simulation of the thermally perfect gas model, the choke limit is reached earlier than in the ideal gas model calculation. At the design point, a total pressure ratio of 2.75 and a mass flow rate of 0.192 kg/s is achieved. The observation of the polytropic efficiency in Figure 6 (b) is comparable. A slightly higher efficiency is achieved in the calculations with thermally perfect gas. As stated in the previous illustration of the mean line distribution of the temperature in Figure 7 (b), a lower value at the outlet of the compressor stage leads to a higher efficiency. The comparison between the calculated gas models and between the two approaches with the thermally perfect gas using the speed lines shows that the simulation with constant pressure results in a significantly larger surge limit distance in the centrifugal compressor stage. This is extremely useful in actual high-temperature heat pump operation in order to operate the plant reliably.

Mean Line Distribution

The results shown in this section are assessed at an operating point close to the surge limit. For this operating point, a static back pressure of 9.27 bar is set at the outlet of the compressor stage. The 1D mean line distribution shown in Figure 7 is derived from the 3D flow solution by mass flow averaging. Figure 7 (a) shows the characteristic of the specific heat capacity over the relative flowpath length. It can be seen very clearly that the simulations with ideal gas model indicate,

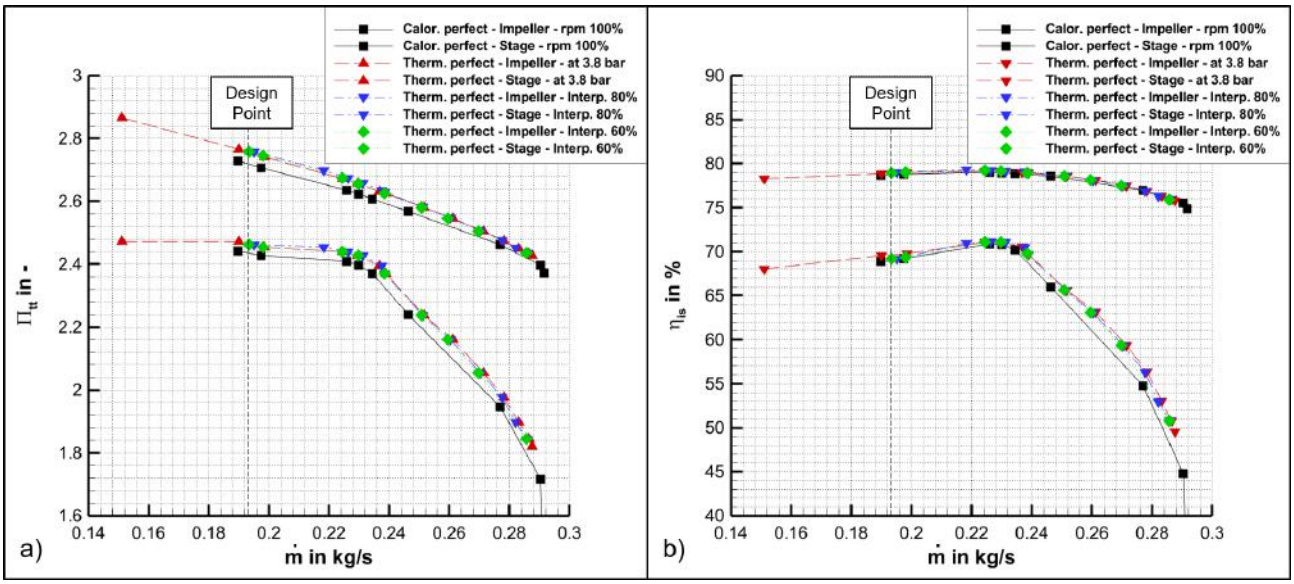

Figure 6 Total Pressure Ratio (a) and Efficiency (b) over the Mass Flow Rate of the Compressor Stage.

as expected, a constant value for the heat capacity over the entire computational domain. In this simulation setup, the constant value is determined from the gas constant R and the isentropic exponent γ and is is around 1,970 J/kg/K. When considering the flow solution computed with the polynomials at a constant pressure of 3.8 bar, a decreasing gradient of the heat capacity over the flow path is observed. This is due to the temperature increase caused by the impeller and results in a reasonable trend compared to the steam tables. Since the temperature in the outlet is almost constant, the heat capacity value there is also constant. The deviation between the value of the ideal gas model shows a maximum positive offset of 300 J/kg/K at the inlet and 80 J/kg/K at the outlet. The analysis of the flow solution with the interpolated polynomials initially indicates a similar trend between the starting pressure of 3.8 bar and the final pressure of 10 bar compared to the heat capacity characteristic calculated at a constant pressure. The inlet of the centrifugal compressor stage gives the same values. A variation occurs in the direction of the flow path of the computational domain. There, the drop in heat capacity is less significant and the magnitude value is higher compared to the constant pressure. This can also be observed in the steam tables, where the progression diverges less rapidly at an efficiency of 80 %. A difference of 70 J/kg/K in heat capacity is found between the two computations with the thermally perfect gas model. The higher level and trend of the heat capacity demonstrate a very accurate conformity of the interpolation from the steam tables. The temperature is also considered over the relative flow path. This shows that the temperature in the outlet area is 20K lower in both calculations with a thermally perfect gas model compared to the calculation with ideal gas Figure 7 (b). The entropy increase, which is generated by

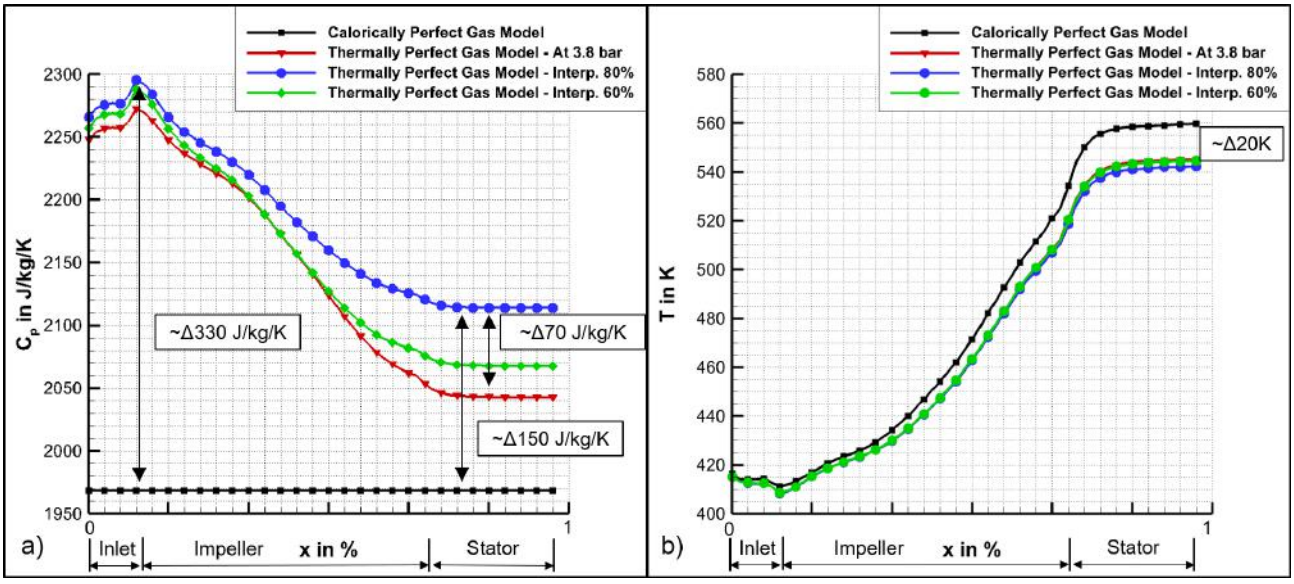

Figure 7 Mean Line Distribution of the Heat Capacity (a) and Temperature (b) over the relative Flowpath Length.

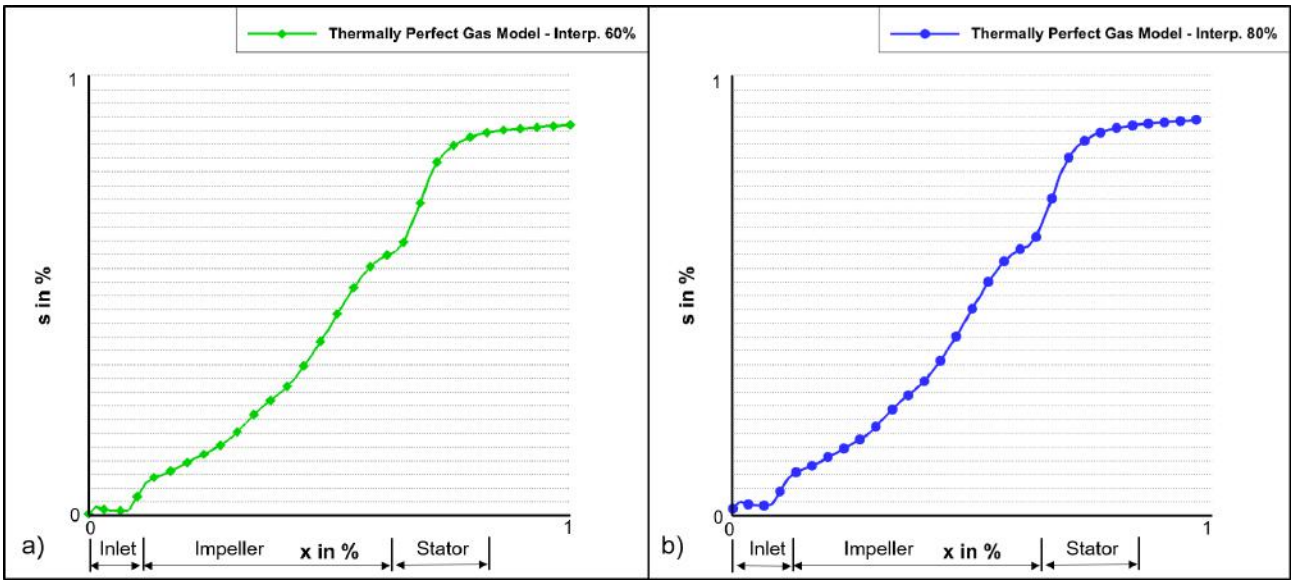

Figure 8 Mean Line Distribution of the Entropy for 60 % (a) and 80 % (b) polytropic efficiency Interpolation.

the energy transfer of the stage to the fluid and flow and friction losses, is also considered. Figure 8 shows the mean line distribution of entropy over the relative flow channel for the flow solution at 60 % (a) and 80 % (b) polytropic efficiency interpolation. The graph indicates that a relatively constant entropy increase occurs within the compressor. The flow in the vaned diffuser reaches its maximum entropy increase. The gradient is at its highest there. Since no energy input into the fluid is possible there, it can be concluded that the flow and friction losses are high in this location. This also indicates the differences in the compressor parameters in the compressor maps when considering the ratios between the impeller and the entire stage in Figure 6. A comparison of the two results shows a very comparable progression of the entropy increase. Consequently, there is no significant difference in the selection of the polytropic efficiency for the interpolation of the state change.

Flow Distribution at constant Blade Height

To conclude, the flow solution is observed using a 2D distribution at a constant blade height of 50 %. The distribution of the specific heat capacity illustrated in Figure 9 shows that the seven polynomial coefficients determined by the interpolation also represent a temperature and pressure dependence in the 3D flow solution. The distribution of the specific heat capacity illustrated in the figure shows that the seven polynomial coefficients determined by the interpolation also represent a temperature and pressure dependence in the 3D-RANS CFD simulation. As is to be expected and can also be seen in the

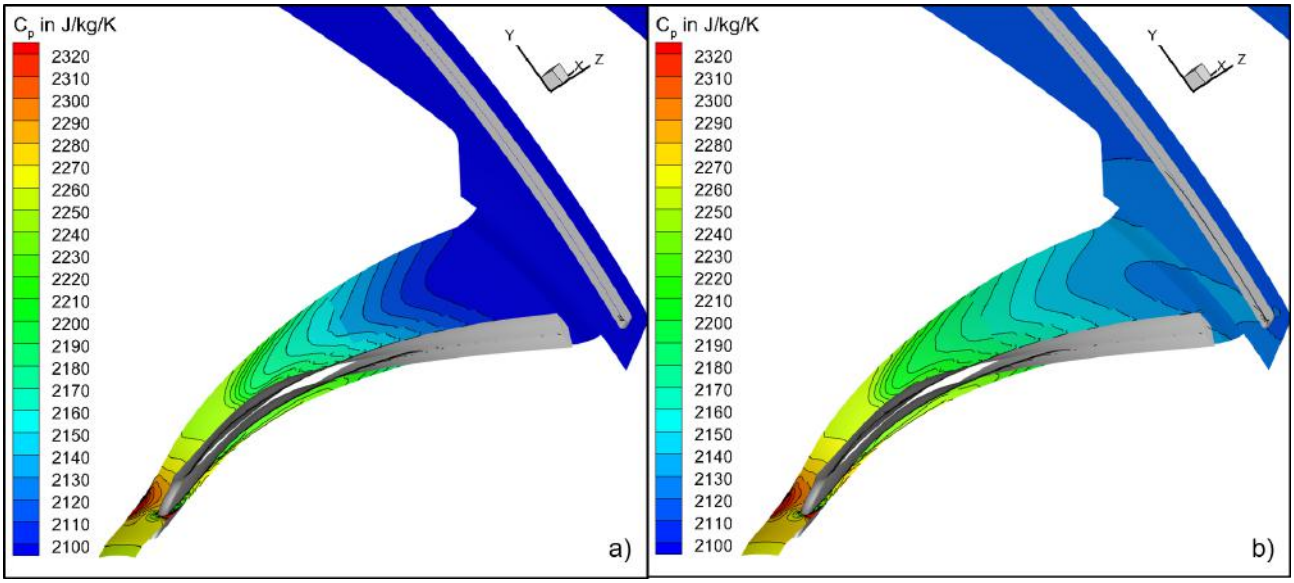

Figure 9 S1 Cut at 50 % Blade Height for 60 % (a) and 80 % (b) polytropic efficiency Interpolation.

mean line distribution of the specific heat capacity, the value of the specific heat capacity after the impeller and in the vaned diffuser is approx. 50 J/kg/K smaller in the calculation with 60 % interpolation than in the simulation with 80 % polytropic efficiency. The distribution of the specific heat capacity demonstrates that further investigation of the fluid mechanical parameters is required to identify more precise variations compared to the existing thermally perfect and ideal gas model. Furthermore, it is essential to compare and validate the numerical results with experimental data.

CONCLUSIONS

The numerical investigations of a centrifugal compressor stage presented in this paper are the results of 3D-RANS CFD simulations carried out with steam as the working medium and calculated and evaluated with the calorically and thermally perfect gas model.

For the thermally perfect gas model used, seven polynomial coefficients are determined by interpolating the steam table values between two pressures and provides a representation of temperature and pressure-dependent modelling of the gas properties.

The comparison of the flow solutions leads to faster choking of the stage at a mass flow of 0.29 kg/s through the vaned diffuser in the simulations with the calorically perfect gas model.

When comparing performance maps such as total pressure ratio and isentropic efficiency over the operating range of the impeller and stage, the thermally perfect gas model shows better results in both evaluation ranges. Up to 0.05 points more in total pressure ratio and up to 0.7 percentage points more in efficiency are calculated.

To enable the modelling of steam as a working medium within CFD simulations, an improvement of the approach is being pursued to be able to compute the optimum matching of the gas properties.

The validation of the numerical results with experimental data is to be conducted on a three-stage HTHP pilot plant and is the objective of ongoing work.

NOMENCLATURE

Greek Letters

η	Efficiency	–
κ	Isentropic Exponent	–

Roman Letters

a	Polynomial Coefficient	–
c_p	Specific Heat Capacity	$\frac{\mathrm{J}}{\mathrm{kg}*\mathrm{K}}$
COP	Coefficient of Performance	–
D	Compressor Geometry Dimensions / Diameter	mm
h	Specific Enthalpy	$\frac{\mathrm{J}}{\mathrm{kg}*\mathrm{K}}$
L	Compressor Axial Length	mm
p	Pressure	bar
R	Gas Constant	$\frac{\mathrm{J}}{\mathrm{kg}*\mathrm{K}}$
s	Specific Entropy	$\frac{\mathrm{J}}{\mathrm{kg}*\mathrm{K}}$
T	Temperature	K
y	Dimensionless First Wall Coordinate	–

Superscripts amd Subscripts

1	States at Inlet	–
2	States at Outlet	–
is	Isentropic states	–
m	Meridional Plane	–
p	Polytropic states	–

ACKNOWLEDGMENTS

We would like to thank the German Aerospace Center DLR, Energy Programme Directorate for its support.

REFERENCES

Acree, W. E. and Chickos, J. S. (2023), 'Phase transition enthalpy measurements of organic and organometallic compounds', *Eds. P.J. Linstrom and W.G. Mallard, National Institute of Standards and Technology, Gaithersburg MD, 20899* **NIST Chemistry WebBook, NIST Standard Reference Database Number 69**.
URL: *https://doi.org/10.18434/T4D303*

Arpagaus, C., Bless, F., Uhlmann, M., Schiffmann, J. and Bertsch, S. S. (2018), 'High temperature heat pumps: Market overview, state of the art, research status, refrigerants, and application potentials', *Energy* **152**, 985–1010.

Bell, I. H., Wronski, J., Quoilin, S. and Lemort, V. (2014), 'Pure and pseudo-pure fluid thermophysical property evaluation and the open-source thermophysical property library coolprop', *Industrial & Engineering Chemistry Research* **53**(6), 2498–2508.
URL: *http://pubs.acs.org/doi/abs/10.1021/ie4033999*

Burcat, A. and Ruscic, B. (2005), 'Third millennium ideal gas and condensed phase thermochemical database for combustion with updates from active thermochemical tables', *Argonne National Laboratory* .

Casey, M. and Robinson, C. (2021), *Radial Flow Turbocompressors: Design, Analysis, and Applications*, Cambridge University Press, UK.

Fedkiw, R. P., Merriman, B. and Osher, S. (1996), 'High accuracy numerical methods for thermally perfect gas flows with chemistry', *Journal of Computational Physics* **132**, 175–190.

Ferziger, J. H. and Perić, M. (2002), *Computational Methods for Fluid Dynamics*, Springer Berlin.

Franke, M., Kügeler, E. and Nürnberger, D. (2005), 'Das dlr-verfahren trace: Moderne simulationstechniken für turbomaschinenströmungen', *DGLR-Jahrbuch. Deutscher Luft- und Raumfahrtkongress* .

Frenklach, M., Bowman, T. and Smith, G. (n.d.), 'Gri-mech'.
URL: *http://combustion.berkeley.edu/gri-mech/index.html*

Grigull, U., Straub, J. and Schiebener, P. (2012), *Steam Tables in SI-Units*, Springer Science & Business Media.

Kajasa, B., Nicke, E. and Kügeler, E. (2023), 'Numerical investigation of a thermally perfect gas model for a centrifugal compressor design with water vapor as working medium', *Proceedings of the ASME Turbo Expo 2023* .

Menter, F. R. and Rumsey, C. L. (1994), 'Assessment of two-equation turbulence models for transonic flows', *25th AIAA Fluid Dynamics Conference* .

Pörtner, H.-O. (2022), 'Ipcc 2022: Impacts, adaptation and vulnerability', *Intergovernmental Panel on Climate Change* .

Roache, P. J. (1994), 'Perspective: A method for uniform reporting of grid refinement studies', *Journal of Fluids Engineering* **116 No. 3**.
URL: *https://doi.org/10.1115/1.2910291*

Slater, J. W. (2022), 'Examining spatial (grid) convergence', *National Aeronautics and Space Administration* **Version 1.0**.
URL: *https://www.grc.nasa.gov/WWW/wind/valid/tutorial/spatconv.html*

Wagner, W., Cooper, J. R., Dittmann, A., Kijima, J., Kretzschmar, H.-J., Kruse, A., Mares, R., Oguchi, K., Sato, H., Stöcker, I., Sifner, O., Takaishi, Y., Tanishita, I., Trübenbach, J. and Willkommen, T. (2000), 'The iapws industrial formulation 1997 for the thermodynamic properties of water and steam', *Journal of Engineering for Gas Turbines and Power* **122**.

APPENDIX A - COPYRIGHT/OPEN ACCESS

APPENDIX B - GPPS Presenter Policy and Paper Acceptance

According to GPPS's presenter attendance policy, a paper cannot be published or be indexed and may not be cited as a published paper until at least one author pays the registration fee and attends the conference. The GPPS reserves the right to withdraw from its publications any paper not presented by an author of the paper at the appropriate conference. Any paper that is withdrawn may not be cited as a published paper.